Chemical Engineering Journal 430 (2022) 132935

Contents lists available at ScienceDirect

Chemical Engineering Journal

journal homepage: www.elsevier.com/locate/cej

Concentration on demand – A microfluidic system for precise adjustment of the content of single droplets

Damian Zaremba, Slawomir Blonski, Piotr M. Korczyk *

Institute of Fundamental Technological Research, Polish Academy of Sciences, Pawinskiego 5B, 02-106 Warsaw, Poland

ARTICLE INFO

Keywords:
Droplet-based microfluidics
Microfluidic traps
Droplet manipulation
Concentration tuning
Concentration gradient

ABSTRACT

We present a novel microfluidic system that produces the required concentration of a reagent in a single droplet or that produces a sequence of droplets with a defined periodic distribution of concentrations. We use digital algorithms that, through a series of simple operations, such as merging and splitting droplets, ensure superior precision, repeatability and flexibility in concentration setting.

Unlike Digital microfluidic (DMF) systems based on electrowetting on dielectric (EWOD) commonly used to implement digital algorithms in the droplet world, our approach is based on much more available channel-based microfluidics operated by programmable syringe pumps. Furthermore, the small footprint of our system makes it easy to integrate with other structures of microfluidic networks. Thus, this technique is a comprehensive component that can be built into the microfluidic networks executing laboratory analytical tasks in chemistry or biology to enrich their performance and offer new functionalities.

1. Introduction

Droplet microfluidic techniques enable the formation and analysis of droplets, each equivalent to a tiny reactor that can include samples, reagents, or biological components for chemical synthesis, analytical assays, biological processes, drug discovery, and more. In these and other applications, obtaining the concentration of a given component in a precise, accurate, and above all, reproducible manner is paramount [1].

This requires a method for the manipulation of the content of droplets. For this purpose, Digital microfluidic (DMF) systems based on electrowetting on dielectrics (EWODs) provide superior control methods for manipulating droplets within multistep and complex handling protocols [2]. Each droplet can be seen as a digital entity, addressed individually and processed with a sequence of merging and splitting selected droplets. EWOD-based DMF systems exploit electrowetting effects that rely on modulation of the interfacial energy of a polar liquid that is deposited on a solid surface by an external electric field. The surface where droplets are processed is coated with individually operated electrodes. A water droplet moves to the electrode in its vicinity that has the highest electric field magnitude. Individual control over the electrodes enables the implementation of liquid handling protocols comprising merging, mixing, and splitting droplets. Although the basic set of operations is strictly limited, the application of digital algorithms offers freedom of concentration creation by using multiple repetitions of primitive operations [3,4] (like a basic computation performed by an algorithm in computer science such as assigning a value to a variable, comparing two numbers, indexing into an array, calling a function/method and returning from a function/method). Thanks to computer-aided systems controlling the electrodes, complicated and reconfigurable procedures can be automatically conducted. However, this technology also presents some limitations. Droplets are in contact with the substrate, and in sliding on its surface can leave some residue, which can result in cross-contamination. Compared to the soft lithography or micromachining commonly used to fabricate conventional channel microfluidic chips, the fabrication of EWOD chips is much more complicated. Operation of the numerous electrodes requires custom electrical connections and custom hardware that demand specific electronics knowledge and skills of their designer.

This disadvantage renders EWOD technology less available to researchers. Fast and relatively cost-effective prototyping techniques for channel microfluidics, such as micromachining, lithography, and 3D printing, are popular. In addition, channel microfluidics has developed various strategies for manipulating the content of droplets that are alternatives to EWOD-based methods. Channel technologies can utilize single-phase gradient generators to prepare concentration before the

* Corresponding author.
E-mail addresses: dzaremba@ippt.pan.pl (D. Zaremba), sblonski@ippt.pan.pl (S. Blonski), piotr.korczyk@ippt.pan.pl (P.M. Korczyk).

https://doi.org/10.1016/j.cej.2021.132935
Received 30 July 2021; Received in revised form 17 September 2021; Accepted 5 October 2021
Available online 16 October 2021

droplet formation or adjust the concentration of a droplet via merging and splitting of droplets with different content.

Droplets with varied concentrations can be achieved by combining the streams of two or more droplet liquids before droplet generation [5]. Mixing takes place after the formation of a droplet due to internal advection [6]. This design allows for the droplet concentration to be varied by adjusting the input liquid ratio while fixing the total flow rate of the droplet phase to ensure monodispersed droplets. Alternatively, droplets of constant size and varying concentrations can be obtained using a fixed-volume droplet generator [7]. More advanced automated systems allow for the choice of the droplet phase from numerous sources [8], or the proportions of composites can be actively tuned by a system of integrated valves [9]. A well-defined spectrum of concentrations can be prepared before droplet generation in a tree-like network that interchangeably splits and combines streams of buffer and reagent within a cascade of junctions. Thus, multiple parallel branches are dedicated to specific output concentrations. Then, each separate output stream is combined with a droplet generator to produce droplets of different concentrations [10,11].

Another category of channel-based microfluidics encompasses systems that rely on the liquid exchange between droplets of different concentrations via series of droplets fusion and fission. Some such systems conduct a series of mass exchanges between a droplet of reagent and a series of input buffer droplets. As a result, the reagent concentration decreases gradually within the stream of resultant droplets. Two different approaches can be applied to serial dilutions - with reagent droplets immobilized [12–14] or moving [13,15,16] while the buffer droplets move or are stopped in the array of traps, respectively. The concentration can be changed gradually in a single droplet by a series of coalescences with small droplets so that the entire volume increases [17]. Dilutions can also be performed in minimalist, iterative systems [18].

While serial dilutions produce series of droplets with gradually distributed concentrations, more control on the individual droplet concentration can ensure merging selected droplets of different liquids. The final concentration is then equal to the proportion of input reagent droplet in the total volume of the resultant droplet. Thus, manipulating the droplet volumes or the number of droplets enables the adjustment of the resultant droplet concentration. This can be done in passive systems [19,20]. Nevertheless, better control over the composition of a single droplet is ensured by active systems supported by the droplet on demand methodology. Individual droplets are made on demand with computer-controlled actuators, so the resultant concentration can be set by adjusting the volumes of constituent droplets [21,22] or their numbers [17]. Similar methods can be adopted to control the number of cells in droplets [23].

Most advanced controlled droplet microfluidic systems allow for iterative operations in oscillatory systems. Here, a train of droplets can be seen as a memory stack. Its controlled motion positions a selected droplet where it can be analyzed by sensors [24–26] or processed, e.g., by an auxiliary junction that removes part of the droplet or adds a portion of a new liquid [27]. Other researchers use addressable static droplet arrays [28].

Such channel-based systems exhibit a level of complexity of operations like that reached in EWOD-based DMF systems. However, the increased complexity of protocols is achieved at the cost of increased complexity of active controller systems. This hampers the wide use of these methods by researchers focused on solving biological or chemical problems who require comprehensive and robust tools without hardware development.

Here, we propose a minimalist channel-based semiautomatic system for precise concentration control whose performance is ensured with digital algorithms. The device's semiautomatic character is due to the use of passive elements such as the metering trap and the merging trap we described above. Therefore, processes such as droplet formation, merging, and splitting do not require any modulation of flows or pressures. Instead, they proceed spontaneously if basic conditions such as the flow direction are met. Thus, the operation is conducted solely by the setting of flows between selected points in the microfluidic setup. The flows are controlled by switching the syringe pumps connected to the channels on or off. The syringes are operated by the time-based controller implemented in software with simple feedback from the camera to track droplets and maintain their position.

Our system exhibits its minimalist character in two aspects. First, the microfluidic structure is relatively small and simple; it consists of only one metering trap and one merging trap, and in the extended dual version, one more merging trap. Second, we use syringe pumps (one per liquid, one additional 3/2 valve in the dual system) as the only actuators in the system that are controlled by the computer software. In this work, we use the auxiliary high voltage electrodes, which are not an intrinsic part of the system but are used only to facilitate droplets' coalescence in the presence of surfactant.

Previously, combinations of microfluidic traps were applied to generate a series of 2-fold dilutions. Here, we propose implementing advanced iterative algorithms, where a so-called beaker droplet can be serially mixed with either a buffer or a reagent droplet, averaging the concentrations of both constituents. This either decreases or increases the initial beaker-droplet concentration in each step of the procedure.

Our procedure exhibits the advantages of both channel-based concentration-control approaches we discussed above without sharing their limitations. First, serial dilution can produce any small concentration, but the resolution of the concentrations in the middle of the range is limited by the fold-number characterizing dilutor. For example, in a 2-fold dilutor, we obtain the first dilution equal to half of the initial concentration, but we cannot obtain any more concentrations greater than half. Similarly, concentrations between a quarter and half of the range are not accessible.

In coalescence-based methods, we have freedom of concentration setting in the middle of the range by tuning the volumes of merged droplets of two liquids. However, in the vicinity of both range limits, this approach requires the precise generation of appropriately small droplets, but the minimum droplet size is determined by the channel dimensions, which introduces a limited concentration adjustment.

We show that our approach is free from those limitations, offering a superior dynamic range within the whole range of concentrations. We analyze the mathematical features of the algorithms used and create the method for generating streams of droplets with concentrations that vary periodically or streams of droplets with the same concentration distribution. We show the practical application of this method for the generation of varying combinations of two reagents in a stream of droplets.

We show that advanced digital algorithms can be effectively implemented in channel systems that are simpler in fabrication and use than EWOD-based DMF systems. Moreover, with its small footprint and minimal set of actuators, the presented solution is suitable as a submodule that can be easily integrated with other modules on a chip device in a lab.

2. Discussion and results

2.1. Mathematical description of the operations on droplets

2.1.1. Averaging of concentration

The concept of the system for control of the concentration in droplets is based on the utilization of a set of base operations on droplets as i) generating droplets of uniform size, ii) merging two droplets, iii) mixing the content of resulting long droplet, and iv) splitting the long droplet into two uniform-sized droplets.

Such a simple set of basic operations can produce droplets containing a combination of two base liquids in any required proportions [4].

The merging of two uniform-sized droplets and mixing of their content results in an averaging of their concentrations. After splitting a double-sized droplet in two, we obtain two unit-sized droplets of

identical concentration. One of the resultant droplets can be used to repeat the operation to modify its concentration.

The droplet being processed in such a way is the *beaker-droplet*, the droplet used to modify the concentration of the *beaker-droplet* is the *input droplet*, and the excess droplet after splitting is the *output droplet* (see Fig. 1a).

The *input droplet* is made directly with one of two base liquids: i) clear solvent or ii) base solution of the reagent. Normalizing the concentration of input droplets by the base reagent concentration, we obtain the dimensionless concentration of the input droplets m, which equals 0 or 1 for the droplet without and with a reagent, respectively. Consequently, the normalized concentration of the reagent in the beaker droplet c can take a value from 0 to 1. Therefore, the base solution of the reagent sets the maximal reagent concentration that can be obtained via droplet combinations.

Let us consider the series of consecutive concentration modifications. The i-th step of the operation can be described as follows:

$$c_i = \langle c_{i-1}, m_i \rangle = (c_{i-1} + m_i) \cdot 2^{-1} \tag{1}$$

where c_i is the concentration of the beaker droplet after the i-th modification, c_{i-1} is the concentration obtained in the previous step or particularly for $i = 1$, $c_{i-1} = c_0$, where c_0 is the concentration of the initial beaker droplet, m_i is the concentration of the input droplet used in the current step, and $\langle , \rangle$ represents averaging. As m_i can be 0 or 1, a single modification can lead to a decrease or increase in the concentration c_i, respectively.

Note that for $i > 0$, the concentration of the i-th output droplet equals the concentration of the beaker droplet c_i. In the following, we will use c_i to describe both the beaker droplet and the output droplet concentration except c_0, which is reserved for the initial beaker droplet concentration only.

We can express c_i as a sum of a geometric series:

$$c_i = c_0 \cdot 2^{-i} + \sum_{k=1}^{k=i} m_k \cdot 2^{(k-i-1)} \tag{2}$$

In general, the initial beaker-droplet concentration c_0 can be any real value from 0 to 1. For example, it can be the residue of the previous sequence of operations.

However, when starting the operation from scratch, c_0 can be 0 or 1, as the initial droplet can be made of one of the base liquids. Thus, in the first step ($i = 1$), we can produce a concentration of 0.5, averaging droplets of different kinds ($\langle c_0 = 0, m_1 = 1 \rangle = \langle c_0 = 1, m_1 = 0 \rangle = 0.5$). In the second step, we have more possibilities, as we can obtain $c_2 = 2 \cdot 2^{-2}$ or $c_2 = 3 \cdot 2^{-2}$ using $m_2 = 0$ or $m_2 = 1$, respectively. In the third step, the tree of all possibilities has four branches representing an additional four intermediary concentrations ($1 \cdot 2^{-3}$, $3 \cdot 2^{-3}$, $5 \cdot 2^{-3}$, $7 \cdot 2^{-3}$ - see Fig. 1b). Therefore, limiting our exemplary series of operations to three steps of modifications, we can obtain any concentration from the spectrum of nine different concentrations given by $A \cdot 2^{-3}$, where A is an integer from 0 to 2^3.

Generally, starting from scratch and within n steps, we can generate any concentration c given by:

$$c = A \cdot 2^{-n} \tag{3}$$

where A is an integer from 0 to 2^n. Hence, increasing the number of steps increases the resolution of the spectrum of available concentrations.

2.1.2. Concentration on demand

For any concentration given by $c = A \cdot 2^{-n}$ and an arbitrarily chosen c_0 (0 or 1), there is a unique sequence of input droplets that can be described as a series of zeros and ones:

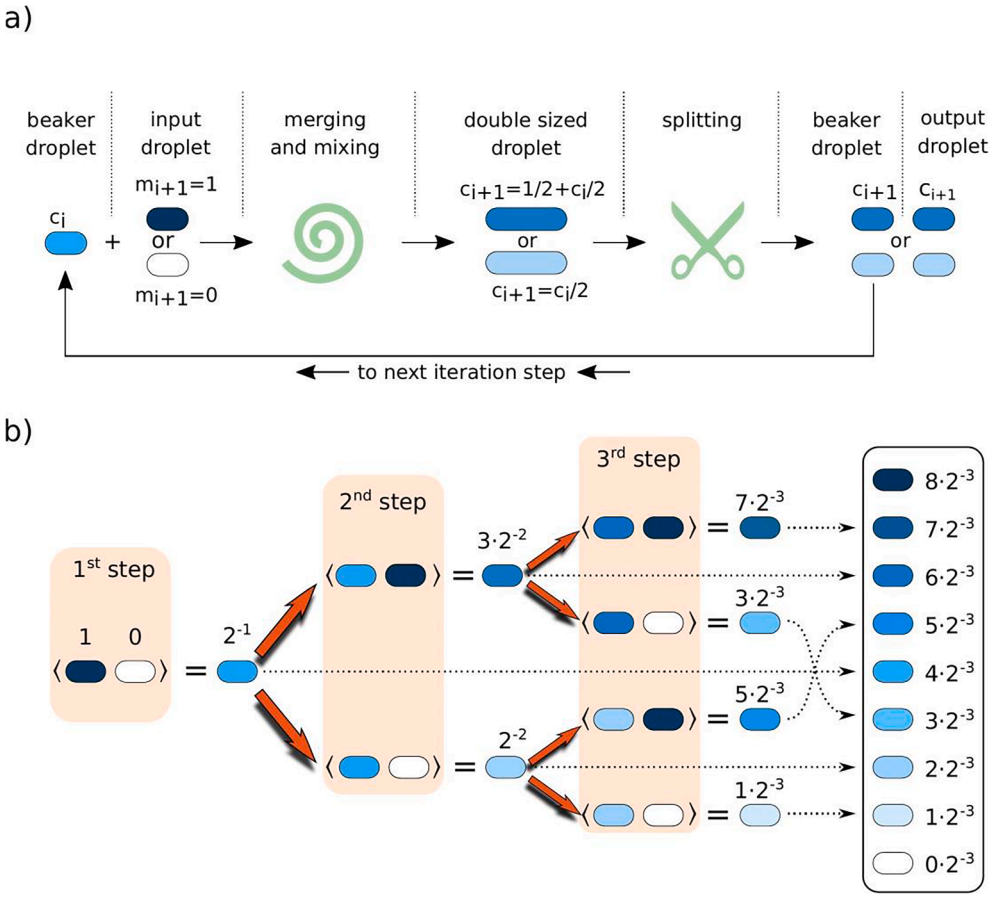

Fig. 1. Concept of the operation on the concentration of droplets. a) Schematic representation of one step of the algorithm for manipulating the concentration by merging and splitting of droplets. The image shows two possibilities – the initial concentration of the beaker droplet c_i is modified through the coalescence with an input droplet of the concentration $m_{i+1} = 1$ or $m_{i+1} = 0$. b) Tree of all possible merge-and-split-operations and resultant concentrations obtained after applying three steps of droplet combinations.

$$\boldsymbol{m}(c_0, c) = [m_1, \ldots m_\nu] \tag{4}$$

Such a series is an instruction required for the generation of the desired concentration c. The length of the input sequence ν is equal to n only if A is an odd number. Otherwise, we can express the concentration as:

$$c = \phi \cdot 2^{-\nu} \tag{5}$$

where $\phi = A \cdot 2^{-(n-\nu)}$ is not divisible by 2. For example, in the case of $c = 6 \cdot 2^{-3}$, $n = 3$ and $\nu = 2$, we can reduce the exponent: $c = 3 \cdot 2^{-2}$. This means that $c = 6 \cdot 2^{-3}$ is obtained in 2 steps (see Fig. 1b).

Having the complete input sequence $\boldsymbol{m}(c_0, c)$ as given in Eq. (4), the final concentration can be calculated from Eq. (2), substituting $i = \nu$:

$$c = c_0 \cdot 2^{-\nu} + \sum_{k=1}^{k=\nu} m_k \cdot 2^{(k-\nu-1)} \tag{6}$$

2.1.3. Reversal problem

An important task for the application of the procedure is to find the input sequence $\boldsymbol{m}$ for any desired concentration c_{desired} described according Eq. (5) by coefficients ϕ and ν as $c_{\text{desired}} = \phi \cdot 2^{-\nu}$. One can use Eq. (6) to calculate the whole tree of resultant concentrations for all possible $\boldsymbol{m} = [m_1, \ldots m_\nu]$ sequences and finally find the unique $\boldsymbol{m}$ giving c_{desired}. However, this method is ineffective, especially for large values of ν. To find the input sequences $\boldsymbol{m}$ for any c_{desired}, the simplest way is to use Eq. (1) to find all intermediate steps starting from the target concentration $c_\nu = c_{\text{desired}}$ and moving step by step back.

From Eq. (1) we have the following formula for the previous-step concentration:

$$c_{i-1} = 2c_i - m_i \tag{7}$$

Starting from $i = \nu$ and $c_\nu = c_{\text{desired}}$, we can guess value m_ν having in mind that for any i, all intermediate concentrations c_i can only have values from 0 to 1. The value of m_ν that satisfies that condition can be 0 or 1 and depends only on the known value c_ν. According to Eq. (7), we have two possible situations: if $c_\nu < 0.5$, m_ν should be 0; otherwise, $c_{\nu-1}$ would be less than 0; and if $c_\nu > 0.5$, m_ν should equal 1; otherwise, $c_{\nu-1}$ would exceed 1. This applies for any step of the sequence i within the interval from $i = 2$ to $i = \nu$, so we can write:

$$m_i = \begin{cases} 0 & if \quad c_i < 0.5 \\ 1 & if \quad c_i > 0.5 \end{cases} \tag{8}$$

which is equivalent to the following equation:

$$m_i = 1/2(1 + sgn(c_i - 1/2)) \tag{9}$$

Starting from the target value c_ν, the value of m_ν comes from Eq. (8) or Eq. (9). Then, putting c_ν and m_ν into Eq. (7) we obtain $c_{\nu-1}$ which is used as the input to Eq. (8) for the estimation of $m_{\nu-1}$. We can repeat that operation until we obtain m_2 and $c_1 = 0.5$. The value of m_1 depends on the arbitrarily chosen c_0.

2.1.4. Approximation of any concentration

In practice, the desired concentration c_{desired} is generally a real number. To use the above algorithm, we first need to use the following approximation:

$$c_{\text{desired}} \approx c_{\text{approx}} = A \cdot 2^{-n} \tag{10}$$

where the accuracy of the approximation is set by the number n and equals 2^{-n}.

The first step is to set the arbitrary resolution of the concentration approximation determined by the coefficient 2^{-n}. Then, we estimate A as rounded value of the product $c_{\text{desired}} \cdot 2^n$ and estimate c_{approx} using Eq. (10). If A is the even number, we replace it (as described above) by an odd number ϕ (see Eq. (5)) yielding $c_{\text{approx}} = \phi \cdot 2^{-\nu}$. Then, we can use the above described algorithm (Eq. (7) and Eq. (8)) to find the input droplet sequence that produces the concentration c_{approx} closest to c_{desired}.

2.2. Implementation in a microfluidic device

2.2.1. Concentration averaging module

The concept of the concentration averaging module (CAM) is based on the use of microfluidic traps described previously [13,29]. As shown in the case of the DOMINO device [13] and the precise dilutor [18], a serial combination of two elements, a metering trap (Fig. 2a) and a merging trap (Fig. 2b), can be used for serial dilutions.

Both traps are composed of slit bypasses along both sides of the channel and obstacles in the lumen of the channel (Fig. 2a and 2b). The metering trap consists of one obstacle, which results in diodicity – the behavior of a droplet depends on the direction of its motion through the trap. The metering trap does not affect droplets entering the trap through the obstacle side, but it influences droplets when they are moving in the opposite direction. That effect depends on the droplet size. A long droplet disassembles into two parts: i) a droplet of the size precisely defined by the trap dimensions that is immobilized in the trap, and ii) an excess droplet that continues traveling [13,29]. All droplets of a size not exceeding the trap dimensions stop in the trap when entering from the unobstructed side. Due to their diodicity, droplets immobilized in the metering trap can be easily released by flow reversal.

The metering trap is used for the metering of base size droplets. That size is determined by the geometry of the trap and hardly depends on the flow or liquid properties (see Supplementary Materials for more details on the measurements of droplets size dependence on the rate of flow). For all operations and specified liquids, we establish fixed parameters of flows at the start of the algorithm. Therefore, the metering trap can be used for precise formation of uniform-sized droplets.

Despite the similar construction of both traps, the merging trap exhibits other functionalities. It immobilizes a droplet of the base size (or smaller) regardless of the flow direction. Due to the symmetry of the trap, which possesses two barriers, after a droplet enters the trap interior, it cannot pass the trap barriers again.

However, in this case, the height of the barriers is smaller than those in the metering trap. The effect is that the merging trap cannot either cut or immobilize longer droplets. For example, double-sized droplets can pass through the trap unaffected. This trap configuration is used to merge pairs of droplets. Once the first droplet is immobilized, the next droplet entering the trap collides and coalesces with the initially immobilized droplet. The resultant double-sized droplet leaves the trap.

In previous publications [13,18], a serial composition of the metering trap and the merging trap was used to generate serial 2-fold dilutions, where the sample was gradually diluted in a cascade of repetitive dilution operations. As a result, the available concentrations were limited and could not be customized at will.

Here, we use a similar composition of traps to develop the semi-automatic system – concentration averaging module, which can execute the algorithm described in section 2.1, allowing for the generation of any required concentration in a small droplet. The base operation of the device is averaging two droplets of identical size by merging them, homogenizing their content and splitting them back into two droplets.

The concentration averaging module consists of the metering trap, the merging trap and the bent section of the channel serving as a mixer [30], all serially connected via a channel (see Fig. 2c). The base size of droplets used in the averaging operation is set by the length of the metering trap. Consequently, the size of the merging trap is adjusted to allow for the immobilization of single-sized droplets and prevent the stoppage of double-sized droplets.

It is important that the metering trap is placed with its barrierless side toward the merging trap. In the module's orientation shown in Fig. 2c, the metering trap does not affect droplets moving from the left.

Let us consider a beaker droplet of concentration c_i introduced to the CAM and stored in the merging trap (Fig. 2c). Now, we send the input droplet from the left with concentration $m_{i+1} = 0$ or $m_{i+1} = 1$ (see Fig. 2d). The input droplet carried by the flow of CP passes the metering trap and then merges with the beaker droplet in the merging trap. The

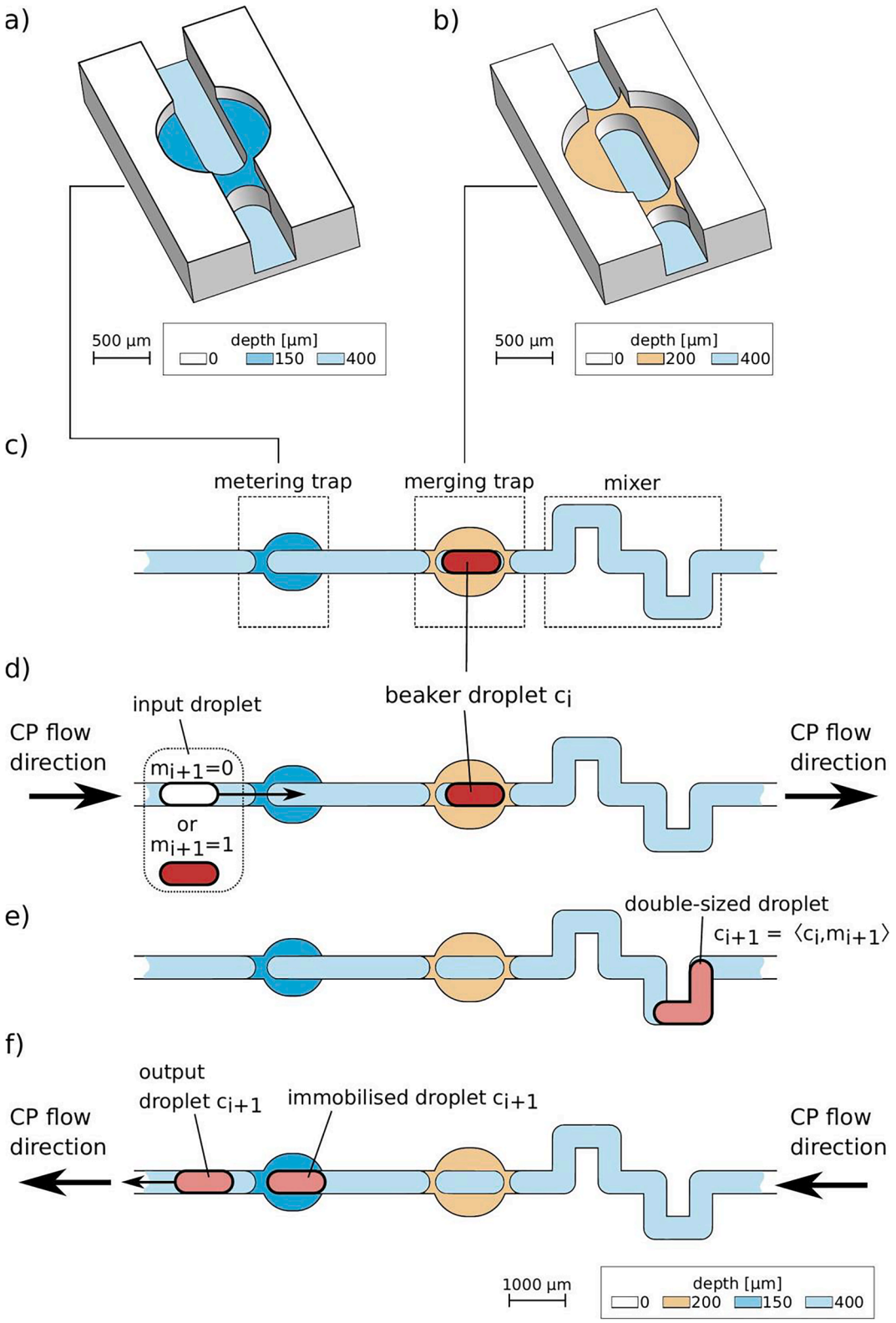

Fig. 2. Concept and operating principles of the microfluidic concentration averaging module. a) and b) 3D schemes of a) metering trap and b) merging trap. c) Concentration averaging module scheme consisting of metering trap, merging trap and bent section of channel serving as a mixer, all serially connected via a channel. In the default configuration, the module contains a single-sized beaker droplet of concentration c_{i-1}. d) In the first step of the operation the direction of the flow is from the left to right and one input droplet of the concentration $m_i = 0$ or $m_i = 1$ is introduced. The input droplet moves toward the trapped beaker droplet. Droplets meet in the merging trap and merge creating a double-sized droplet, which leaves the merging trap and travels through the mixer, homogenizing the content to the concentration $c_i = (c_{i-1} + m_i)/2$ - (e). Then, the flow is reversed. The double sized droplet passes through the merging trap and is divided into two droplets of the same size and concentration c_i - (f) in the metering trap. One of the droplets continues traveling to the left, while the other one is trapped in the metering trap.

resultant double-sized droplet leaves the merging trap and travels through the channel's bends (see Fig. 2e), which facilitates homogenization of the content by enforcing irregular internal convection. As a result, according to Eq. (1), the mixing of the two collided droplets yields a double-sized droplet of concentration $c_{i+1} = (c_i + m_{i+1}) \cdot 2^{-1}$. Then, the flow direction is reversed, and the double-sized droplet passes the merging trap and enters the metering trap, where it divides into two equal droplets of the base size (see Fig. 2e). One droplet (the output droplet) leaves the module, while the second droplet (the beaker droplet) stays inside the module. Thus, the module is ready for the next input droplet to alter the beaker-droplet concentration further.

The above-mentioned operation scheme assumes the perfect mixing and homogenization of the content of the double-sized droplet after merging two droplets of different concentrations. The mixing in the droplet proceeds due to the internal circulation forced by the confined flow conditions. For this purpose, the distance that double-sized droplet travels from its creation to its splitting is ensured sufficiently long – 13.4 of the double-sized droplet lengths. Additionally, the mixing is enhanced by the bendings [30] of the mixer zone what ensures the required homogenization of the droplet content.

2.2.2. Droplet on demand module

The implementation of the algorithm described in section 2.1 requires the delivery in each step of an input droplet of solvent or droplet of reagent, selected according to the demand of the algorithm. Here, we propose a novel and simple Droplet On Demand system (DOD), which utilizes the metering trap (see Fig. 3a).

The main part of the module is a metering trap connected via the channel and tubing directly to a DP syringe that is operated by a bidirectional syringe pump. Importantly, the metering trap is oriented with the barrier side directed toward the DP inlet. Thus, it can meter a droplet when the flow is from right to left (according to the layout in Fig. 3). The additional channel expansion prevents the spontaneous formation of unwanted droplets.

The syringe pump operating such a DOD system must work in both directions – in the injection and withdrawal modes.

In the base position of the DOD, the DP fills the whole tubing, and the tip of the DP is in the channel between the inlet and the metering trap (see Fig. 3b I). In the first stage of DOD module operation, the droplet phase is pumped forward until its tip passes the whole metering trap (see Fig. 3b I-IV). Therefore, the DP fills the whole input channel, the channel expansion and the metering trap (Fig. 3b IV). In the next step, the syringe pump works in withdrawal mode which forces the flow from right to left (see Fig. 3b V-VI), and the tip of the DP moves to the left. As a result, a droplet forms in the metering trap. Further withdrawal of DP increases the gap between the DP and the droplet immobilized in the trap. This gap is filled with CP. Then, the injection of DP moves the droplet from the trap, and the device is ready for the generation of the next droplet.

This procedure does not require any calibration and is simple in operation, requiring only a sequence of flow reversals. Therefore, it resembles the push-and-release procedure in hand pipettes.

The volume of droplets produced in our DOD system is about 114nL. The high reproducibility of the formed droplets is confirmed by the small relative standard deviation of droplet size measurements estimated in the series of repetitions to be about 1.5%.

2.2.3. Concentration on demand module

We integrated both CAM and DOD modules shown in sections 2.2.1 and 0, obtaining the functional Concentration on Demand Module (CDM - see Fig. 4). What is important and beneficial is that the device's design includes only one metering trap shared between the modules. Thus, the device consists of one metering trap, one merging trap, and the inlet of the CP connected to the mixer side of the CAM. The output is placed between the channel expansion of the DOD and the metering trap. Two inputs of different droplet phases are connected directly to the expansion of the DOD.

Each liquid is managed by a dedicated bidirectional syringe pump controlled by the computer. The custom-made software drives switching sequences of syringe pumps in different configurations, inducing flows

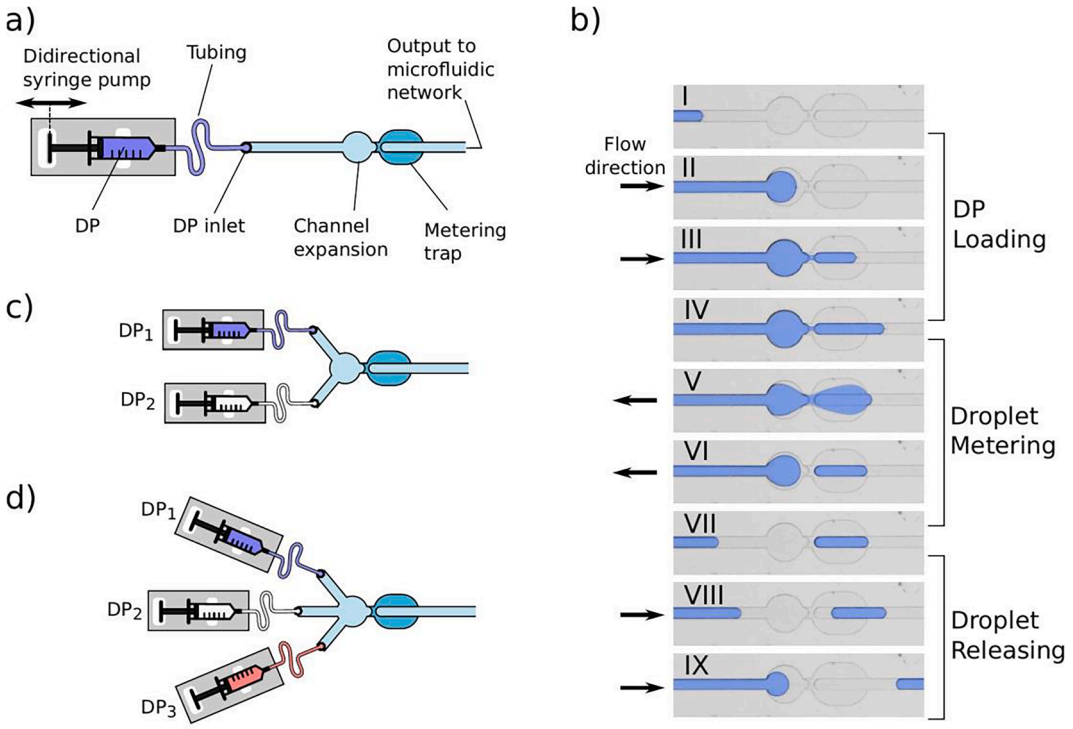

Fig. 3. Droplet on demand module with the metering trap. a) Scheme of the microfluidic module and its connection to the bidirectional syringe pump with DP, b) experimental images showing the working device and subsequent stages of operation of DOD, c), d) examples of extended DOD modules for the generation of droplets of different droplet phases, c) DOD module with two different droplet phases DP_1 and DP_2, and d) configuration of DOD for three different DPs: DP_1, DP_2, DP_3.

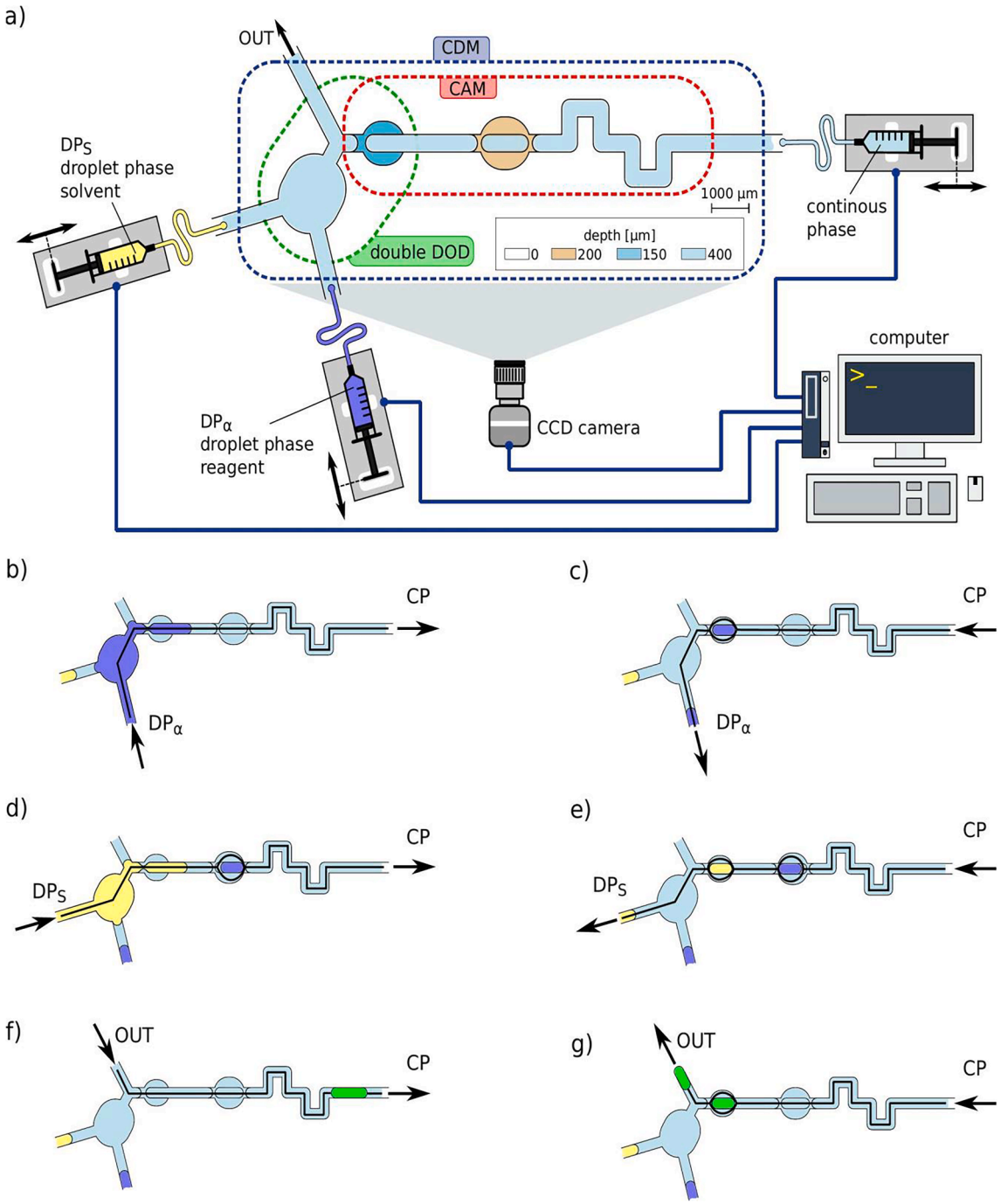

Fig. 4. Concept of the automated concentration on demand module and its operating principles. a) Scheme of the microfluidic CDM and diagram showing connections to three bidirectional pumps. Pumps and CCD camera observing the system are connected to a computer and operated by the software which executes the algorithms and b) – g) schematic representation of all base operations of CMD for performing the complete Concentration on Demand algorithm.

between selected points of the microfluidic device (see Fig. 4b–g). In this way, the CDM executes the algorithms described above autonomously and automatically.

Two droplet phases used in the CDM encompass the base reagent solution, here called DP_α, and the solvent DP_S.

Let us analyze the CDM principles in the schemes shown in Fig. 4b–g. In the beginning, DP_α is injected into the system, while the flow of CP is reversed by the withdrawal mode of the CP syringe pump. The induced flow is between the DP_α inlet and the CP inlet (see Fig. 4b). This stage encompasses the loading of DP_α into the DOD as described before in Section 0 (see Fig. 3 II-III). Once the tip of DP_α is detected behind the metering trap, the previous flow pattern is reversed, i.e., the DP_α syringe pump is switched to withdrawal mode, while the CP is run in the forward mode. As a result, a single droplet of DP_α is created and immobilized in the metering trap, and the tip of DP_α recedes and hides in the DP_α inlet channel (see Fig. 4c).

In this paper, we use a digital camera to detect the DP tip presence behind the metering trap. Then, the feedback signal from the camera is used by the operating software to reverse the DP's flow once the DP fills the metering trap. Importantly, the flow reverse must occur before the DP tip enters the merging trap. We chose the distance between traps arbitrarily long enough to avoid biases due to possible delays in the feedback system.

The analogical process performed using the DP_S syringe pump in

place of the DP_α syringe pump leads to the creation of a DP_S droplet in the metering trap (see Fig. 4d and 4e). The DP_α droplet produced previously in the metering trap moves to the merging trap during DP_S injection into the DOD system.

Finally, two single-sized droplets, the beaker droplet and the input droplet, occupy the merging tap and the metering trap, respectively (see Fig. 4e). Then, the flow of CP switched in reverse mode removes the droplet from the metering trap and merges it with the other droplet in the merging trap. The resultant double-sized droplet's content is homogenized as it travels through the mixer (see Fig. 4e). Then, after switching the CP syringe to forward mode, the double-sized droplet divides in the metering trap into equal parts. The output droplet leaves through the outlet, while the second droplet, the beaker droplet, remains trapped in the metering trap. Finally, the system is ready for the next step of the algorithm, where through the operations described above, a droplet of DP_α or DP_S is created and collides with the beaker droplet.

Thus, the presented system performs all operations required for the execution of the Concentration on Demand algorithm.

2.2.4. Experimental verification

We tested a real microfluidic CDM fabricated in polycarbonate (see SM device 1) that was aimed at the generation of concentrations predicted by Eq. (6). We produced all concentrations that are available in 4 steps of the algorithm, which together with varied concentrations of base liquids yielded 17 different concentrations.

Using the procedure described in section 2.1.3, we estimated the sequences of input droplets for each concentration, shown symbolically in Fig. 5 as rows of dark and white droplets. Then, the computer-aided system performed the appropriate operations. The images of the resultant droplets show a smooth transition of blue dye intensity for droplets put in their concentration order. Movie 1 shows the example of the generation of a droplet with a concentration of 0.4375.

In additional experimental runs, the concentration was measured (see Methods). The results were plotted in a graph. Both the color dye visualization and quantitative estimation of the concentration show agreement with the mathematical predictions.

2.3. Periodical sequences of droplet

2.3.1. Theoretical description

Previously, we focused on setting the concentration of one beaker droplet. The procedure described included the retraction of output droplets as an excess in each step of the iterative algorithm.

Now we focus on the output droplets. Hence, we can see the device as a numeric filter that processes the sequence of our input droplets and produces a series of excess droplets.

We show that periodicity in the input signal results in periodicity of the output signal, enabling the periodic generation of concentrations in droplets.

Let us assume the periodicity of the input sequence of carrier droplets:

$$m_{i=p\cdot\omega+s} = \pi_s \tag{11}$$

where ω is the length of a single period (number of droplets in a single period). p is the number of complete periods. $s \in [1, \omega]$ is a droplet's position within the period and can be described in terms of the modulo operation:

$$s = [(i-1) \bmod \omega] + 1 \tag{12}$$

$\boldsymbol{\pi} = [\pi_1, \pi_2, \ldots, \pi_\omega]$ is a vector containing ω elements which define the periodic input pattern.

Substituting $i = p\cdot\omega + s$ to Eq. (2) gives:

$$c_{p\cdot\omega+s} = c_0 \cdot 2^{-(p\cdot\omega+s)} + 2^{-(s+1)} \left(\frac{1-2^{-p\cdot\omega}}{2^\omega - 1} \sum_{\sigma=1}^{\omega} 2^\sigma \pi_\sigma + \sum_{\sigma=1}^{s} 2^\sigma \pi_\sigma \right) \tag{13}$$

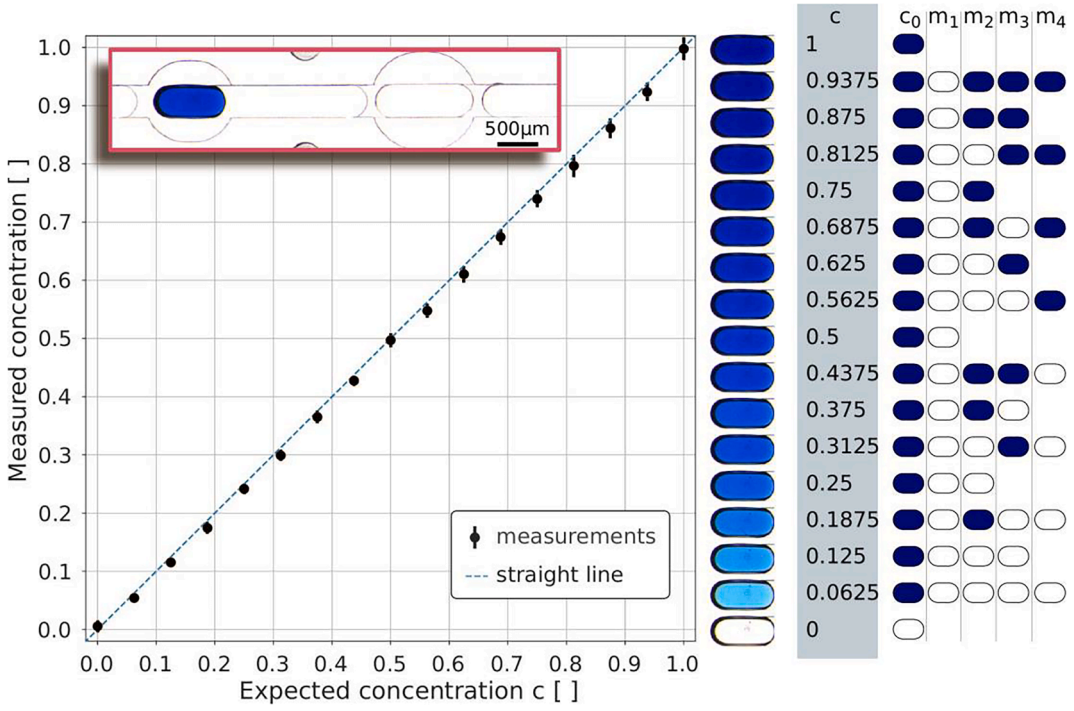

Fig. 5. Experimental verification of the microfluidic module for concentration manipulations. The graph shows the results of experimental runs, where we produced all 17 possible concentrations for 4 steps of the algorithm. For each concentration, at least 10 repetitions were performed. Plotted points indicate the mean value of the measurements (with error-bars indicating standard deviations of measurments) and the corresponding images of droplets show the visualization obtained from the dissolution of blue dye in water. The inset shows a section of a microfluidic device with a beaker droplet inside. Images of droplets in column right show a smooth transition of blue dye according to the expected concentration. Column c lists all expected concentrations in order. The rows of dark and white droplets symbolize the sequences of input droplets used to generate each corresponding concentration.

The terms with $2^{-p\cdot\omega}$ quickly vanish with increasing $p\cdot\omega$ so that the dependency on both c_0 and p disappears, yielding:

$$\lim_{i\to\infty} c_{i=p\cdot\omega+s} = \eta_s = 2^{-(s+1)}\left(\frac{1}{2^{\omega}-1}\sum_{\sigma=1}^{\omega} 2^{\sigma}\pi_{\sigma} + \sum_{\sigma=1}^{s} 2^{\sigma}\pi_{\sigma}\right) \tag{14}$$

Thus, Eq. (14) defines a periodic output pattern $\boldsymbol{\eta} = [\eta_1, ..., \eta_\omega]$ of a length equal to the length of the input pattern $\boldsymbol{\pi}$.

In summary, if an input sequence $\boldsymbol{m}$ is the repetition of the base pattern $\boldsymbol{\pi}$: $\boldsymbol{m} = [\boldsymbol{\pi}, \boldsymbol{\pi}, \boldsymbol{\pi}, ...]$, the output for large i is periodic and converges to a periodic stream of droplets

$$\boldsymbol{\zeta} = [\boldsymbol{\eta}, \boldsymbol{\eta}, \boldsymbol{\eta}, ...] \tag{15}$$

where $\boldsymbol{\eta} = [\eta_1, ..., \eta_\omega]$ is given by Eq. (14).

Note that the vanishing dependence on the initial concentration implies that the periodic series is stable against perturbations. Indeed, the initial concentration c_0 can be seen as a perturbation if there is any error. We can see that the system quickly restores the defined periodic sequence.

2.3.2. *Examples of experimental runs for periodic patterns*

To clarify the periodicity of output droplets, we consider two examples of periodic input patterns:

$$\boldsymbol{\pi} = [0, 1] \tag{16}$$

and

$$\boldsymbol{\pi} = [0, 1, 0, 0, 0, 1, 0, 1, 1, 1] \tag{17}$$

The first example uses the simplest nontrivial pattern (Eq. (16)) with length $\omega = 2$. Repeating this pattern, we produce the input sequence $\boldsymbol{m}$, where the concentration of all odd input droplets is 0 and the concentration of all even input droplets is 1:

$$m_{p\cdot 2+1} = 0, m_{p\cdot 2+2} = 1 \tag{18}$$

Let us analyze the periodicity of the output assuming $c_0 = 1$. Eq. (13) yields:

$$c_{p\cdot 2+s} = 2^{-(p\cdot 2+s)} + 2^{-(s+1)}\left(\frac{1-2^{-p\cdot 2}}{3}4 + \sum_{\sigma=1}^{s} 2^{\sigma}\pi_{\sigma}\right) \tag{19}$$

For odd droplets (s = 1), the output is:

$$c_{p\cdot 2+1} = \frac{1}{3} + \frac{4^{-p}}{6} \tag{20}$$

For even droplets (s = 2), the output is:

$$c_{p\cdot 2+2} = \frac{2}{3} + \frac{4^{-p}}{12} \tag{21}$$

As the number of repetitions of the periodic pattern p increase, the term containing 4^{-p} vanishes in both Eq. (20) and Eq. (21). Thus, the concentration of odd output droplets converges to 1/3, while the concentration of even output droplets converges to 2/3 (see Fig. 6 and Table 1.).

Hence, after an initial transition, the output stabilizes, and the device produces droplets of two well-defined concentrations, resulting in a periodic output stream of droplets with repetition of the pattern:

$$\boldsymbol{\eta} = (1/3, 2/3) \tag{22}$$

The same $\boldsymbol{\eta}$ as in Eq. (22) we obtain applying Eq. (14) to pattern $\boldsymbol{\pi}$ given in Eq. (16).

In the next example, we consider a periodic input pattern of length $\omega = 10$ and of the form $\boldsymbol{\pi} = [0, 1, 0, 0, 0, 1, 0, 1, 1, 1]$. Applying Eq. (14) to this pattern, we obtain the following periodic output (see Fig. 7 and Table 2.):

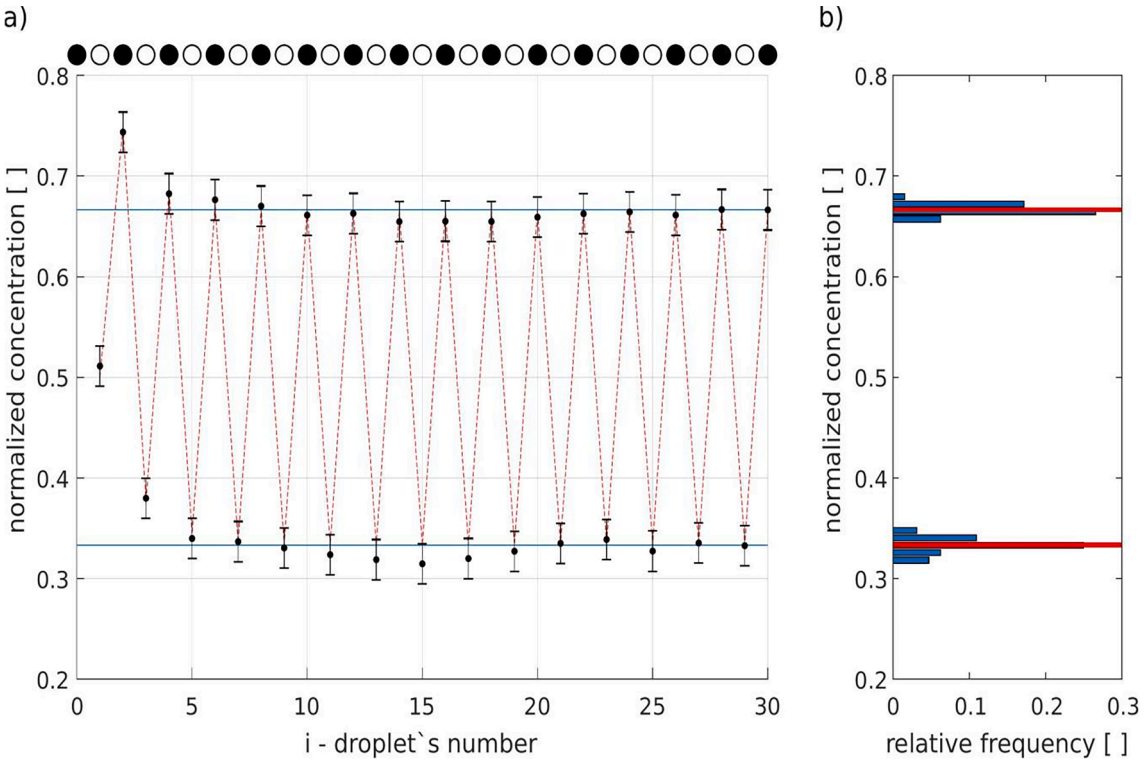

Fig. 6. Measurements of the concentration of output droplets for the input sequence $\boldsymbol{m} = (\boldsymbol{\pi}, \boldsymbol{\pi}, \boldsymbol{\pi}, ...)$ consisting of repetitions of the pattern $\boldsymbol{\pi} = (0, 1)$ with the initial $c_0 = 1$. a) Plotted points are measurements based on pixel values from images of the output droplets. The red line connects points of theoretical prediction (Eq. (2)). White and black spots above the plot indicate the concentration of the i-th input droplet (white-filled = 0, black-filled = 1) and b) histogram of measured concentration taken for 65 consecutive droplets after arbitrary output stabilization from the 6^{th} to 70^{th} droplets.

Table 1
Values of i, s, p, m, c, ζ and c- ζ for first 5 periods for the input pattern given in Eq. (16) and $c_0 = 1$. Values of c calculated using Eq. (2) and values of ζ calculated using Eq. (14) and Eq. (15).

i	1	2	3	4	5	6	7	8	9	10
s	1	2	1	2	1	2	1	2	1	2
p	0	0	1	1	2	2	3	3	4	4
m	0	1	0	1	0	1	0	1	0	1
c	0.500	0.750	0.375	0.688	0.344	0.672	0.336	0.668	0.334	0.667
ζ	0.333	0.666	0.333	0.666	0.333	0.666	0.333	0.666	0.333	0.666
c-ζ	0.167	0.083	0.042	0.021	0.010	0.005	0.003	0.001	0.001	0.000

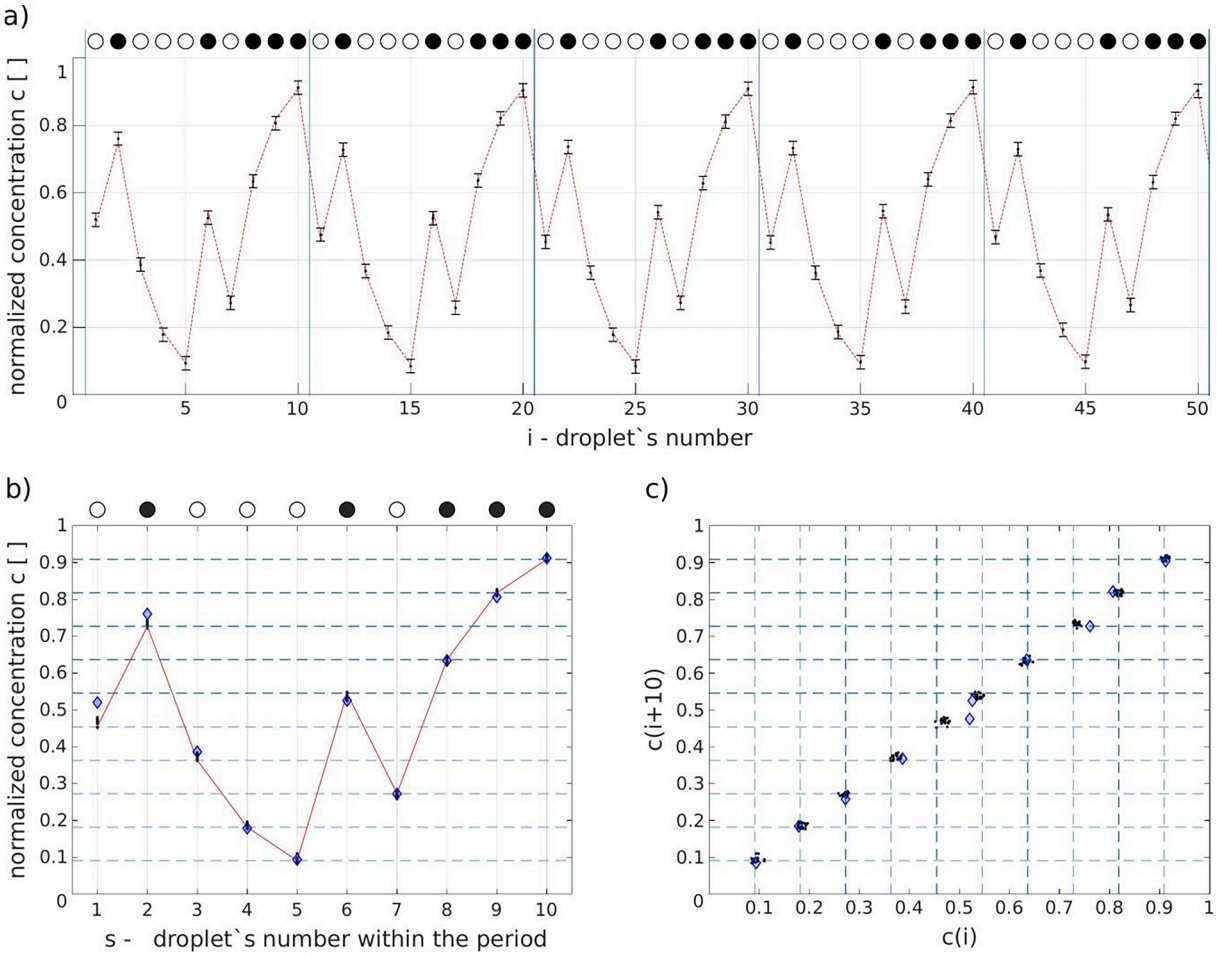

Fig. 7. Experimental analysis of the series of concentrations resulting from the processing of input droplets with the input sequence $\boldsymbol{m} = (\boldsymbol{\pi}, \boldsymbol{\pi}, \boldsymbol{\pi}, \ldots)$ where the periodic pattern is $\boldsymbol{\pi} = (0,1,0,0,0,1,0,1,1,1)$ and initial concentration is $c_0 = 1$. a) Black dots with error-bars: measurements of the concentration of dye for the first five periods of resultant droplets. The single periods are separated by vertical blue lines. The red line connects theoretical points calculated according to Eq. (2), b) data for the sequence of 197 droplets plotted together as a function of $s = [(i-1) \bmod \omega] + 1$: all output periods overlapped by shifting their origins to position 1. The red line connects points calculated according to the periodic solution given in Eq. (14), and c) Poincaré plot: c_{i+10} versus c_i for all 197 droplets showing that each period consists of 10 unique concentrations uniformly distributed. The points from the first period are plotted in b) and c) as blue diamonds.The rest of the measurements are black dots. White and black circles above the plots a) and b) indicate the concentration of the i^{th} input droplet (white = 0, black = 1).

$$\boldsymbol{\eta} = [0.455, 0.727, 0.364, 0.182, 0.091, 0.546, 0.273, 0.636, 0.818, 0.909] \tag{23}$$

Interestingly, in this case, all resultant concentrations are integers (from 1 to 10) multiplied by the concentration equal to $c_{\text{step}} = 0.0909$, so the output pattern can be expressed as follows:

$$\boldsymbol{\eta} = [5, 8, 4, 2, 1, 6, 3, 7, 9, 10] \cdot c_{\text{step}} \tag{24}$$

The experimental analysis shows that the results quickly converge to the periodical series of concentrations. This particular pattern can be used for the generation of concentrations that are linearly distributed.

2.3.3. Linear- and logarithmic-scaled series of concentrations

In the previous example (shown in Fig. 7), we showed that an input sequence given in Eq. (17) of length $\omega = 10$ provides a linear-scaled set of concentrations. We observed that linear-scaled concentrations can be obtained from other input sequences. The prerequisites are that the length of the sequence ω is an even number, and one half of the sequence is the Boolean negation of the second half ($\pi_i = \neg\pi_{i+\omega/2}$). We obtained linear-scaled concentrations, for example, for the sequences $\boldsymbol{\pi} = [0,1]$, $\boldsymbol{\pi} = [1,1,0,0]$ and $\boldsymbol{\pi} = [0,1,0,0,0,1,0,1,1,1]$. However, satisfying the abovementioned prerequisites does not guarantee a linear distribution, and we did not find a general rule.

Table 2
Values of i, s, p, m, c, ζ and c- ζ for first 2 periods for the input pattern given in Eq. (16) and $c_0 = 1$. Values of c calculated using Eq. (2) and values of ζ calculated using Eq. (14) and Eq. (15).

I	1	2	3	4	5	6	7	8	9	10	11	12	13	14	15	16	17	18	19	20
s	1	2	3	4	5	6	7	8	9	10	1	2	3	4	5	6	7	8	9	10
p	0	0	0	0	0	0	0	0	0	0	1	1	1	1	1	1	1	1	1	1
m	0	1	0	0	0	1	0	1	1	1	0	1	0	0	0	1	0	1	1	1
c	0.500	0.750	0.375	0.188	0.094	0.547	0.273	0.637	0.818	0.909	0.454	0.727	0.364	0.182	0.091	0.545	0.273	0.636	0.818	0.909
ζ	0.455	0.727	0.364	0.182	0.091	0.545	0.273	0.636	0.818	0.909	0.455	0.727	0.364	0.182	0.091	0.545	0.273	0.636	0.818	0.909
c-ζ	0.045	0.023	0.011	0.006	0.003	0.001	0.001	0.000	0.000	0.000	0.000	0.000	0.000	0.000	0.000	0.000	0.000	0.000	0.000	0.000

The repetition of serial 2-fold dilutions is natural for the generation of logarithm-scaled sets of concentrations. Note that for the input period $\boldsymbol{\pi}$ containing only a nonzero value at its first position ($\pi_1 = 1$) while containing zeros at the remaining positions ($\pi_{s\neq 1} = 0$), Eq. (14) simplifies to:

$$\eta_s = 2^{-s}(1-2^{-\omega})^{-1} \tag{25}$$

Thus, we obtain a series of consecutive 2-fold dissolutions that uniformly cover the logarithmic scale:

$$\boldsymbol{\eta} = (1-2^{-\omega})^{-1}\cdot\left[2^{-1}, 2^{-2}, ..., 2^{-\omega}\right] \tag{26}$$

Notice that the term $(1-2^{-\omega})^{-1}$ in Eq. (25) for $\omega = 2$ equals 4/3, for $\omega = 3$ equals 8/7, and for further increasing length of the input pattern ω it converges to a value close to unity. For example, for $\omega = 7$, $(1-2^{-\omega})^{-1} = 1.0079$ which less than 1% different than 1.

This means that for $\omega \geq 7$ we can state $(1-2^{-\omega})^{-1} \approx 1$. Thus, the output periodic pattern simplifies to the form

$$\boldsymbol{\eta} \approx \left[2^{-1}, 2^{-2}, ..., 2^{-\omega}\right] \tag{27}$$

In such a case, we can neglect the transient character of the beginning of the output sequence.

2.4. Periodic cross-combinations

2.4.1. The concept

As we show here, the periodic properties of a series of concentrations allow for effective generation of a broad number of cross-combinations of the concentrations of two different reagents.

Let us consider two parallel streams of input droplets, each droplet with varying concentrations of two different reagents represented by α and β, respectively. Assume that those streams are periodic with different periodic patterns $\boldsymbol{\pi}_\alpha$ and $\boldsymbol{\pi}_\beta$ of lengths ω_α and ω_β and produce the sequences $\boldsymbol{c}_\alpha$ and $\boldsymbol{c}_\beta$ of output concentrations with periodic patterns $\boldsymbol{\eta}_\alpha$ and $\boldsymbol{\eta}_\beta$. Colliding pairs of droplets from two independent sequences, we obtain combinations of concentrations $c_{\alpha,i}$ and $c_{\beta,i}$ for each $i-th$ resultant αβ-droplet.

To make the idea clearer, let us consider a simple example with $\omega_\alpha = 2$ and $\omega_\beta = 3$. Let $\boldsymbol{\pi}_\alpha = [1,0]$ and $\boldsymbol{\pi}_\beta = [1,0,0]$ be periodic input patterns (see Fig. 8a), which according to Eq. (14) results in periodic output patterns

$$\boldsymbol{\eta}_\alpha = (4/3)\cdot\left[2^{-1}, 2^{-2}\right] \tag{28}$$

and

$$\boldsymbol{\eta}_\beta = (8/7)\cdot\left[2^{-1}, 2^{-2}, 2^{-3}\right] \tag{29}$$

respectively (see Fig. 8c). For the simplicity, let's assume that the initial concentrations equal the last elements of periodic output patterns ($c_{\alpha,0} = \eta_{\alpha,\omega_\alpha} = (4/3)\cdot 2^{-2}$ and $c_{\beta,0} = \eta_{\beta,\omega_\beta} = (8/7)\cdot 2^{-3}$) what ensures the periodicity of the output concentrations starting from the first droplet, without any initial transition ($\boldsymbol{c}_\alpha = \boldsymbol{\zeta}_\alpha$ and $\boldsymbol{c}_\beta = \boldsymbol{\zeta}_\beta$).

Repeating α pattern ω_β times and β pattern ω_α times, we obtain two periodic sequences, each of the same length $\omega_\alpha\cdot\omega_\beta = 6$ (see Fig. 8d):

$$\boldsymbol{c}_\alpha = \boldsymbol{\zeta}_\alpha = [\boldsymbol{\eta}_\alpha, \boldsymbol{\eta}_\alpha, \boldsymbol{\eta}_\alpha] = (4/3)\cdot\left[2^{-1}, 2^{-2}, 2^{-1}, 2^{-2}, 2^{-1}, 2^{-2}\right] \tag{30}$$

and

$$\boldsymbol{c}_\beta = \boldsymbol{\zeta}_\beta = \left[\boldsymbol{\eta}_\beta, \boldsymbol{\eta}_\beta\right] = (8/7)\cdot\left[2^{-1}, 2^{-2}, 2^{-3}, 2^{-1}, 2^{-2}, 2^{-3}\right] \tag{31}$$

Pairing droplets at the same position i from both sequences creates double-sized αβ-droplets of unique combinations of both reagent concentrations. Thus, we obtain $n_\alpha\cdot n_\beta = 6$ combinations covering the complete spectrum of all possible pairs for 2- and 3-element sets (see Fig. 8e). Note that the final merging of droplets results in an additional single-fold dilution of reagents; thus, the final concentrations in an

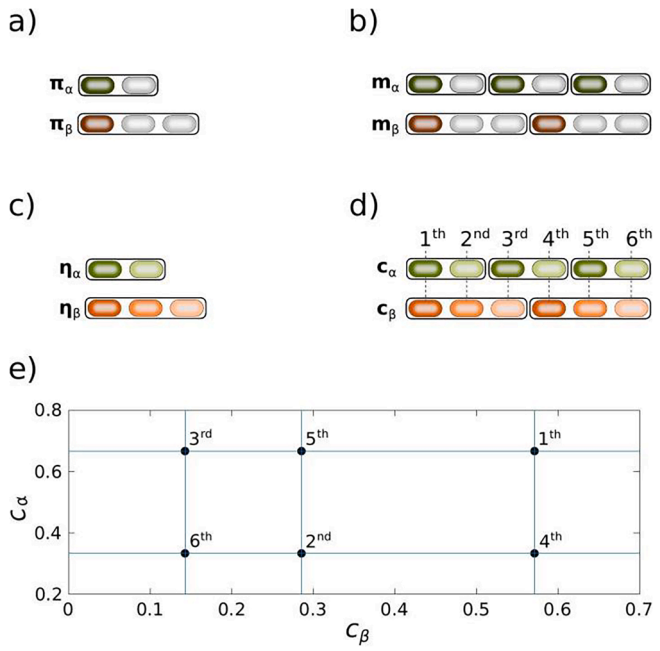

Fig. 8. The concept of cross-combination of concentrations from two periodic sequences. a) Schematic presentation of input periodic patterns $\boldsymbol{\pi}_\alpha = [1,0]$ and $\boldsymbol{\pi}_\beta = [1,0,0]$ of lengths $\omega_\alpha = 2$ and $\omega_\beta = 3$ for two different reagents α and β, respectively. Dark colored droplets contain reagents while the bright colorless ones are of pure solvent, b) two periodic input sequences $\boldsymbol{m}_\alpha$ and $\boldsymbol{m}_\beta$ of $\omega_\alpha{\cdot}\omega_\beta$ elements each, constructed by the repetition of the $\boldsymbol{\pi}_\alpha$ pattern ω_β times and the $\boldsymbol{\pi}_\beta$ pattern ω_α times, c) output period patterns $\boldsymbol{\eta}_\alpha$ and $\boldsymbol{\eta}_\beta$, and d) output sequences $\boldsymbol{c}_\alpha$, $\boldsymbol{c}_\beta$ – repetitions of output period patterns, and e) plot showing all obtained combinations of concentrations c_α, c_β.

αβ-droplet are halves of the concentrations of single-sized droplets: $c_{\alpha,i} = 0.5c_{\alpha,i}$, $c_{\beta,i} = 0.5c_{\beta,i}$. Thus, the maximum concentration that we can reach is half of the maximum concentrations of the input liquids. This should be considered at the design stage of the experiment and preparation of the base concentrations to ensure the desired range of the concentrations in the combined droplets.

This procedure can be used for longer sequences, resulting in a larger number of pairs and denser coverage of the plane of cross-combinations. The prerequisite is that the least common multiple of ω_α and ω_β be equal to their product $\omega_\alpha{\cdot}\omega_\beta$.

2.4.2. Microfluidic implementation of periodic cross-combinations

To execute the abovementioned cross-combinations of sequences, we built a system (see Fig. 9a and SM device 2) that is an extension of the CDM described in Section 2.2.3. The first obvious extension is adding the DP_β input droplet supplying phase with reagent β. Thus, in the Dual-CDM, a triple DOD module replaces the double DOD module previously used in the single CDM version.

The next key difference is the bifurcation of the CP inlet channel into two channels called α-storage and β-storage. These bifurcated ducts extend behind the microfluidic chip in tubing, come together at an external 3/2 solenoid valve, and then connect to the CP syringe pump via common tubing.

The 3/2 valve allows for the active switch of CP flow between the bifurcations. Therefore, the entire CP flow is directed through the currently selected storage channel, while the opposite flow is inactive (with zero flow). These two flow configurations are the two modes of the device.

Fig. 9b and Fig. 9c show the flow patterns and active syringes in both device modes. We can see that those modes functionally represent two single CDMs that are partially overlapped and divergent at the channel's bifurcation.

Each mode, together with its assigned storage channel, is dedicated to processing a single reagent: α or β. The dual-CDM operates similarly to the single device in each of its modes, performing all operations (as described in Section 2.2.3) for each reagent independently.

Reagents cannot be processed simultaneously using the same device, so interchangeable switching of modes is required to perform collision-free sequences by suspending one reagent's processing while the other is being processed.

The algorithm assumes that mode swapping is performed once the double-sized droplet (created after merging the beaker droplet with the input droplet) passes the mixer channel (see Fig. 4f for a reference) and enters the dedicated storage channel. The switching proceeds automatically. The control software detects the appearance of a droplet in the storage channel (thanks to the use of the camera) and changes the setting of the 3/2 valve. Thus, the storage channel receiving the incoming droplet now becomes deactivated, halting the droplet there and suspending its processing until the next mode swap. Simultaneously, that event activates the opposite storage channel, resuming the other reagent's processing starting from when the previous mode swap suspended it. Thus, the double-sized droplet of the other reagent is released from its activated storage channel and continues in the CDM sequence.

Thanks to such a device's configuration, instead of using two independent CDMs, we use only one shared module to generate both sequences of α and β reagents independently. This ensures that a minimal set of traps is used to proceed with the whole algorithm. As a benefit, we use only one metering trap, so all droplets are generated based on its geometry, which avoids any size differences among multiple traps due to fabrication tolerances.

The last modification of the device is an additional merging trap placed in the output channel. The role of this trap is the pairing of droplets from both sequences containing dilutions of different reagents.

The empty trap catches the output droplet of one of the reagents. Due to alternate switching of processed reagents, the next output droplet is made of the other reagent. Thus, a pair of droplets of different reagents meet at the merging trap, forming αβ-droplets of double size that leave the system, emptying the trap for the next pair. As a result, this mechanism pairs and merges every i-th α-droplet with the i-th β-droplet of concentrations $c_{\alpha,i}$ and $c_{\beta,i}$, respectively, creating double αβ-droplets of concentrations $c_{\alpha,i} = 0.5c_{\alpha,i}$ $c_{\beta,i} = 0.5c_{\beta,i}$. Thanks to this design, the pairing of droplets is performed passively simply by taking advantage of the merging trap.

The αβ-droplet can be directed from its output to another section of a microfluidic device for further processing and analysis (e.g., the addition of a bacterial culture). Fig. 9d shows an experimental image from the dual-CDM after the creation of a cross-combined αβ-droplet. That double-sized droplet of color, resulting from the mixing of base colors (red and blue in appropriate proportions), is moving to finally leave the device.

We tested the device and the above-described algorithms on the sequences defined by the following periodic patterns:

$$\boldsymbol{\pi}_\alpha = [0,1,0,0,0,1,0,1,1,1] \tag{32}$$

and

$$\boldsymbol{\pi}_\beta = [0,1,0,0,0,1,0,1,1,1,1] \tag{33}$$

of lengths $\omega_\alpha = 10$ and $\omega_\beta = 11$, respectively. The least common multiple of ω_α and ω_β equals their product $\omega_\alpha{\cdot}\omega_\beta = 110$. Hence, for a fully periodic series, we can obtain 110 unique cross-combinations of concentrations.

Starting the sequence from the scratch (in this case with initial $c_0 = 0$), we should be aware that the initial concentrations of droplets may substantially diverge from the theoretical periodic series; however, by expanding the whole sequence with additional (e.g., 9) droplets, we can recover the periodic values of the first droplets. Starting from the 111^{th} droplet, we initiate the next period, e.g., the 111^{th} droplet is equivalent

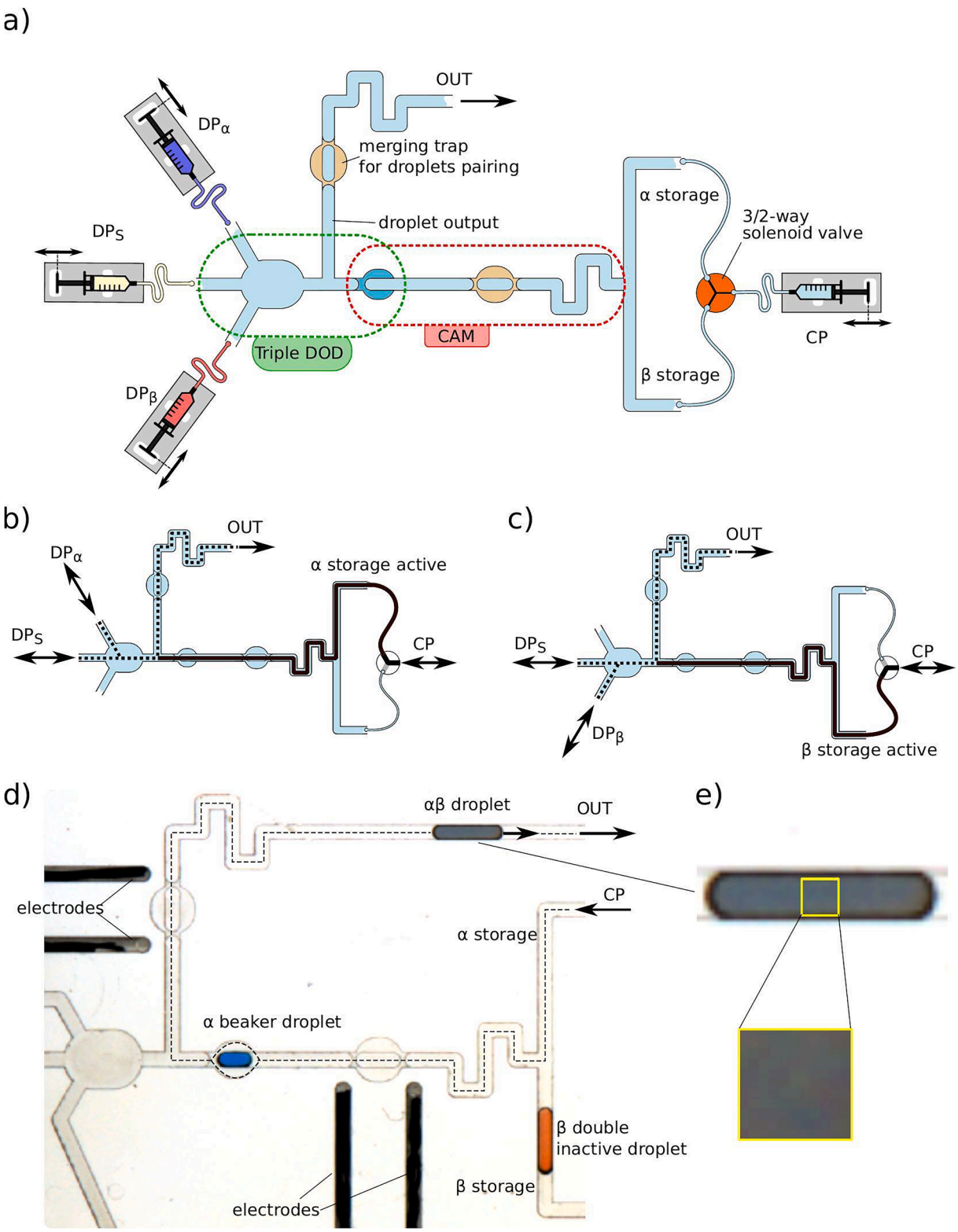

Fig. 9. Dual concentration on demand module. a) Scheme of the microfluidic dual-CDM and diagram showing connections to four bidirectional pumps operating the setup. Pumps are connected to a computer (not shown here) and operated by the software which executes the algorithms, b), c) flow patterns for two settings of the 3/2 valve, b) flow patterns for α-storage active. c) flow patterns for β-storage active, d) experimental image from the running dual-CDM, and e) magnified image of the αβ-droplet with an 11 pixels × 11 pixel square from its interior used to create the collage in Fig. 10b.

to the first droplet of a fully periodic series. The transient initial stage results provide some additional points scattered between the points for a fully periodic solution (see Fig. 10b).

In experimental tests, we used input sequences $\boldsymbol{m}_\alpha = [0, \boldsymbol{\pi}_\alpha, \boldsymbol{\pi}_\alpha, ...]$ and $\boldsymbol{m}_\beta = [0, \boldsymbol{\pi}_\beta, \boldsymbol{\pi}_\beta, ...]$ with initial concentrations $c_{\alpha,0} = c_{\beta,0} = 0$. The additional input droplets with zero concentration at the beginning of the $\boldsymbol{m}_\alpha$ and $\boldsymbol{m}_\beta$ sequences ensure that the first output droplet is made of the solvent only ($c_{\alpha,1} = c_{\beta,1} = 0$), adding the auxiliary reference point in the

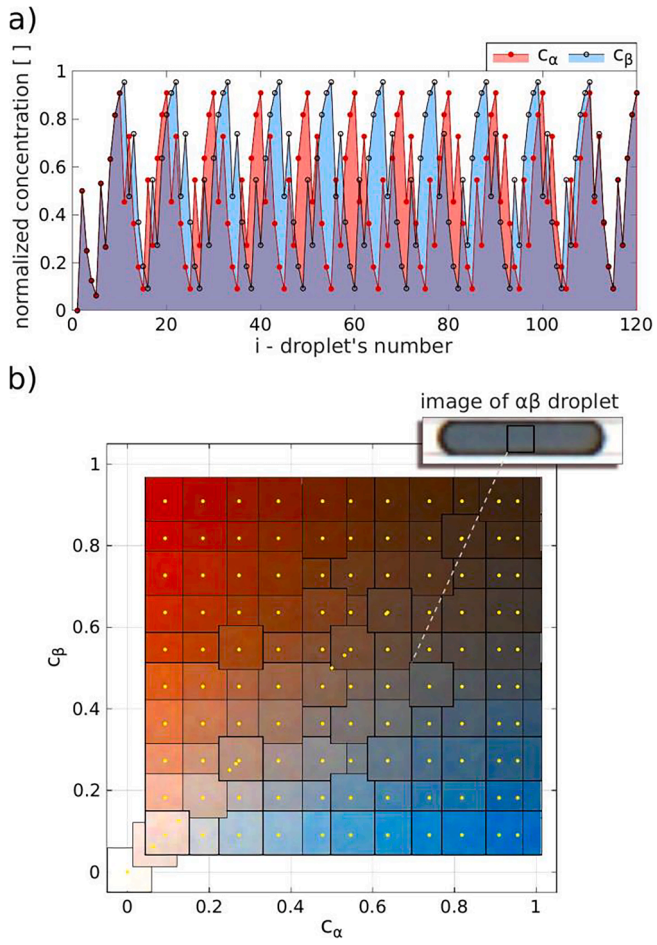

Fig. 10. Experimental examination of the dual-CDM. a) Plots of predicted concentrations $\boldsymbol{c}_\alpha$ and $\boldsymbol{c}_\beta$ resulting from processing the input sequences $\boldsymbol{m}_\alpha = [0, \pi_\alpha, \pi_\alpha, \ldots]$ and $\boldsymbol{m}_\beta = [0, \pi_\beta, \pi_\beta, \ldots]$, where $\boldsymbol{\pi}_\alpha = [0,1,0,0,0,1,0,1,1,1]$ and $\boldsymbol{\pi}_\beta = [0,1,0,0,0,1,0,1,1,1,1]$, calculations made using Eq. (1) and b) diagram showing all possible combinations of c_a versus c_b obtained by combining droplets from two periodic series. The color collage was created by putting 120 squares (11 pixels × 11 pixels), each taken from the interior of experimental images of αβ-droplets (see the inset in the right top corner and Fig. 9e). Images are distributed according to coordinates given by assigned expected output concentrations c_α and c_β (i.e., i-th image occupies the position $c_{\alpha,i}$, $c_{\beta,i}$).

measurement series. Furthermore, as pointed out above, we extended the number of processed droplets with an additional 9 droplets for a total of 120 to recover the periodical results for the first droplets. Movie 2 shows the beginning of the conducted experiment.

We calculated the expected sequences of concentrations $\boldsymbol{c}_\alpha$ and $\boldsymbol{c}_\beta$ by applying Eq. (1) to input sequences $\boldsymbol{m}_\alpha$ and $\boldsymbol{m}_\beta$. The plots of both $\boldsymbol{c}_\alpha$ and $\boldsymbol{c}_\beta$ sequences are presented in Fig. 10a.

Fig. 10b shows the results of the experiments with the Dual-CDM which processed input sequences defined by $\boldsymbol{m}_\alpha$ and $\boldsymbol{m}_\beta$. The base liquids α and β were aqueous solutions of color indicators – blue and red, respectively – while the solvent was clear water. Therefore, every combination of concentrations of both dyes is assigned to the unique color of a droplet.

Fig. 10b shows 120 squares (11 pixels × 11 pixels), each taken from the interior of experimental images of subsequent αβ-droplets (see Fig. 9e and the inset in Fig. 10b). Those images are distributed according to coordinates given by assigned expected output concentrations, creating a collage on the $c_\alpha c_\beta$-plane (i.e., i-th image occupies the position $c_{\alpha,i}$, $c_{\beta,i}$). The smooth color transition in all directions visualizes the correct operation of the device and the validity of the proposed algorithm.

3. Conclusions

In this paper, we designed and built devices that use complex digital procedures to adjust the concentration of reagents within droplets in microfluidic channels. The small device's footprint and minimal sets of actuators (only syringe pumps for the basic variant) render this architecture a comprehensive module that can be built into a larger device for processing a series of further operations on droplets. Moreover, the system shown can work in a variety of configurations. For example, the syringe pump with CP can be connected from the other side and collect excess droplets, as shown in Fig. 4. Each double-sized droplet would potentially be an output droplet, as well. Due to its reconfigurability, a CDM built into a microfluidic network can be adjusted to avoid any disturbance of flows in the rest of the channel systems.

In the presented device, we used the microfluidic traps reported previously as components of microfluidic systems for the production of serial dilutions in droplets [13,18]. Here we show the module composed of the minimal set of traps integrated with the novel DOD system. Unlike previous traps systems, the new device avoids the waste of samples while offering programmable execution of a much more comprehensive range of different laboratory procedures beyond the consecutive dilutions.

As shown, the only mechanical parts are pumps, and the operation of the systems relies on the sequence of their switching actions to forward or backward directions or stopping. Due to passive elements, the system does not require any calibration to achieve satisfactory precision and accuracy. Syringe pumps are quite common, so the proposed technology can be adapted in most laboratories without additional purchases. Most commercial and open-source syringe pumps are available with drivers and libraries, allowing for their control by custom software written in popular environments.

The presented system and algorithms are envisioned to be developed toward better usage of resources. For example, implementing temporal storage for the output droplets would decrease the time and minimize waste in the precise adjustment of the concentration of a single droplet [3]. The simplest way to implement storage is to use a long channel connected to the CDM on one side and to add a pump on a second side. This would realize a stack memory, adding two principal operations to the system: store, which would add a droplet to the collection, and load, which would remove the most recently added droplet. One or more stacks added to the device would convert the device into a stack machine that could execute many other algorithms and be a more general-purpose processor.

Another perspective may emerge from implementations of sequential logic microfluidic circuits, which, with a series of permutations [31], could prepare a required sequence of input droplets. Such systems would produce the encoded distribution of concentrations with passive self-organization of the flow, requiring fewer external manipulations by programmed sequences of flow reversals. This would open the possibility of creating compact microfluidic devices, such as the function generators used in electronics to generate different types of waveforms.

The other interesting aspect of the presented system is that it can be seen as a linear time-invariant system and described as digital signal processing, where the input sequence of droplets can be described as a digital signal. In linear time-invariant systems, convolution of the input signal with the impulse response results in the output signal. The algorithm presented in the paper describes the ideal system. It implements a first-order infinite impulse response filter with constrained coefficients equal to 0.5, which makes it a low-pass filter. The impulse response of the filter is well-known. Unfortunately, in real systems, some imperfections exist, for example, due to fabrication or the constraints of pumps. This can result in systematic differences in generated droplets. Therefore, the impulse response can also be measured in the device to obtain improvements in achieving the demanded concentrations by adding corrections to the described algorithm.

The article presents examples close to linear distributed

concentrations, while logarithmic dilutions are more common in analytical practice. As we mentioned, our system is capable of the preparation of serial dilutions and their cross-combinations for two-reagent systems. Moreover, the logarithmic dilutions are simpler for the implementations in our systems than nonlogarithmic dilutions. We wanted to show less obvious linear-like distributions to emphasize that the presented system is much more flexible in setting different concentrations than simple dilution-based microfluidic systems.

Finally, we show that digital algorithms operating on droplets are not only the domain of EWOD-based DMF systems but can be effective and relatively easily implemented in channel-based microfluidics.

Besides the above-mentioned advantages and novelty, the main shortcoming of our system is the relatively low throughput. Indeed, the hydrodynamic traps require flows with sufficiently low Capillary numbers [29], which is achieved by keeping the flow rate below some critical level, limiting the efficiency.

In the case of the experiments presented in this article, the single step of the algorithm, including sequence of i) generation of a droplet, ii) merging droplets, iii) mixing, and iv) splitting, takes about 19 s. This time can be lowered a few-fold by the further optimization of the device. Still, because of the limit for Capillary number, the efficiency cannot approach the level offered by the high-throughput microfluidic systems [32]. However, this paper aimed rather at the microfluidic system's precision, controllability, automation-ability, and simplicity than at high throughput. Still, the low-throughput offering by our system is not problematic in the potential applications, where the investigated reaction time is relatively long, e.g., amplification of DNA or biological assays involving cell cultures.

As we mentioned before, the proposed system can be developed to implement more advanced algorithms, including memory-like storage of droplets. Additionally, it can be enriched with feedback from the measurements of the reaction in droplets. Thus, searching for the optimal reaction condition can be adjusted in each step and focused on the more narrow range of parameters. Thus, this approach differs from the other titration-like methods requiring high throughput, where the reaction results are scanned through a series of numerous dilutions covering the whole range densely. Our system's ability to implement algorithms based on numerical methods such as, e.g., the bisection method, can increase the efficiency at a minimal number of steps, compensating the operations' low throughput.

4. Materials and methods

4.1. Liquids

We used hexadecane (Sigma Aldrich Co.) with the addition of approximately 0.2% Span 80 (Sigma Aldrich Co.) as CP and 6% or 24% glycerine (Sigma Aldrich Co.) water solution as DP. In all experiments, one syringe was filled with colorless DP, and the others were filled with the same DP with added dye. We used methylene blue (Sigma Aldrich Co.) for experiments presenting single droplet diluters. Food dyes (Allura Red AC (E129) and Brilliant Blue FCF (E133), Sigma Aldrich Co.) were used for the dual-droplet dilution experiment.

4.2. Microfluidic devices

All the presented devices were fabricated by milling geometries in 4- or 5-mm plates of polycarbonate (Makrolon, Bayer AG, Germany) using a CNC milling machine (Ergwind, Poland) with 0.4-mm end mills (FR208, inGraph, Poland). In the case of milled surfaced, the value of the profile roughness parameter is Ra $= 0.742 \pm 0.072$ μm (measured using the Keyence VK-X100 profilometer). The fabricated devices were additionally inspected using a profilometer toward the agreement of the fabricated geometrical details to the design (see Supplementary Information). The contact angle for the milled surface was 104.3° ±2.5° measured using Data Physics OCA 15 goniometer.

After engraving the microfluidic geometries in one plate of PC, the other plate was bonded to close channels. Finally, the device was sealed and had only holes for inlets and outlets. To align both plates in the correct position, we used steel pins inserted into auxiliary holes. An exploded view of a fabricated microfluidic device is shown in Supplementary Material.

The plates were bonded using a hot press at 135° C for 10 min. We applied no further channel modifications. Before the first use, the devices were kept filled with CP for several minutes.

We used additional electrodes to facilitate the coalescence of merging droplets. Electrodes were made from wire (UL3239 28AWG with insulation XLPE, rated voltage 6 kV-DC). We inserted electrodes into dedicated channels to place their ends close to the merging trap where droplets coalescence.

To simplify our experiments, we added a large container at the output (channel with depth and width of at least 3 mm) which collected output droplets. This container's far larger depth than the output channel of the diluter prevented the return of irrelevant droplets to the system when the flow reversed. The container also had two outlets connected to a waste container outside of the microfluidic device. The volume of the tank allowed several hundred superfluous drops to be collected. It allowed each presented experiment to be conducted without a break. The filled container was flushed out manually using one of the outputs connected to the waste container.

4.3. Experimental setup

To control the system, we used syringe pumps (Low Pressure Syringe Pump neMESYS 290 N, Cetoni GmbH, Germany) with 1 ml glass syringes (1001TTL, Hamilton, USA) connected to the inlets of devices via PTFE tubing (S1810-10, Bola GmbH, Germany) with an 0.8 mm inner diameter and a 1.6 mm outer diameter. Tubing was connected to the system with cut needles that were pressed into the input and output holes of the microfluidic system. We used up to four syringe pumps and one 3/2-way solenoid valve (ASCO 067 Rocker, Emerson, USA) controlled through one of the syringe pump modules. Each liquid used in the experiments was acted on by only one dedicated pump. Hence, the number of pumps equaled the number of liquid types. The valve was connected to the syringe with CP and used to change channels that store droplets in the two-droplet mixing experiments.

The use of a surfactant prevented wetting of the channel walls by the DP, disrupting droplets.

Droplets flowing in the investigated microfluidic devices were observed using a stereoscope (HSZ-645TR, Huvitz, South Korea) equipped with a CCD camera (UI-3274LE-C-HQ, IDS, Germany). The camera was used to synchronize transitions and to record images of transitional and final concentrations of droplets. To increase the accuracy of the measurement of methylene blue, we added a bandpass filter of 550 nm – 570 nm in the c-mount of the stereoscope.

4.4. Calibration of the concentration measurements

A calibration curve was measured for experiments where methylene blue was used, and measurements of the concentrations of droplets formed were presented. For this purpose, intermediate concentrations between colorless and colored DP were made manually using a pipetting device. The following concentrations were used: 0, 0.125, 0.250, 0.375, 0.5, 0.625, 0.750, 0.875, and 1. The system was manually filled with each concentration using a syringe. For each concentration, the image brightness was measured at the same location where the image brightness was measured for the measured droplets and the background. As a result, a calibration curve was obtained by fitting a polynomial to the experimental data.

Declaration of Competing Interest

The authors declare that they have no known competing financial interests or personal relationships that could have appeared to influence the work reported in this paper.

Acknowledgements

The project operated within the First Team grant (POIR.04.04.00-00-3FEF/17-00) of the Foundation for Polish Science co-financed by the EU under the Smart Growth Operational Programme. D.Z. acknowledges support within the Preludium grant (UMO-2018/29/N/ST3/01711) of the National Science Centre, Poland. The authors thank dr. Joanna Radziejewska for the help with profilometer measurements.

Appendix A. Supplementary data

Supplementary data to this article can be found online at https://doi.org/10.1016/j.cej.2021.132935.

References

[1] X. Wang, Z. Liu, Y. Pang, Concentration gradient generation methods based on microfluidic systems, RSC Adv. 7 (2017) 29966–29984, https://doi.org/10.1039/C7RA04494A.
[2] E. Samiei, M. Tabrizian, M. Hoorfar, A review of digital microfluidics as portable platforms for lab-on a-chip applications, Lab. Chip. 16 (2016) 2376–2396, https://doi.org/10.1039/C6LC00387G.
[3] S. Roy, B.B. Bhattacharya, K. Chakrabarty, Optimization of dilution and mixing of biochemical samples using digital microfluidic biochips, IEEE Trans. Comput.-Aided Des. Integr. Circuits Syst. 29 (2010) 1696–1708, https://doi.org/10.1109/TCAD.2010.2061790.
[4] S. Bhattacharjee, A. Banerjee, T.-Y. Ho, K. Chakrabarty, B.B. Bhattacharya, Efficient generation of dilution gradients with digital microfluidic biochips, IEEE Trans. Comput.-Aided Des. Integr. Circuits Syst. 38 (2019) 874–887, https://doi.org/10.1109/TCAD.2018.2834413.
[5] J.D. Tice, H. Song, A.D. Lyon, R.F. Ismagilov, Formation of droplets and mixing in multiphase microfluidics at low values of the reynolds and the capillary numbers, Langmuir. 19 (2003) 9127–9133, https://doi.org/10.1021/la030090w.
[6] H. Song, M.R. Bringer, J.D. Tice, C.J. Gerdts, R.F. Ismagilov, Experimental test of scaling of mixing by chaotic advection in droplets moving through microfluidic channels, Appl. Phys. Lett. 83 (2003) 4664–4666, https://doi.org/10.1063/1.1630378.
[7] V. van Steijn, P.M. Korczyk, L. Derzsi, A.R. Abate, D.A. Weitz, P. Garstecki, Block-and-break generation of microdroplets with fixed volume, Biomicrofluidics. 7 (2013), 024108, https://doi.org/10.1063/1.4801637.
[8] F. Gielen, L. van Vliet, B.T. Koprowski, S.R.A. Devenish, M. Fischlechner, J.B. Edel, X. Niu, A.J. deMello, F. Hollfelder, A fully unsupervised compartment-on-demand platform for precise nanoliter assays of time-dependent steady-state enzyme kinetics and inhibition, Anal. Chem. 85 (2013) 4761–4769, https://doi.org/10.1021/ac400480z.
[9] H.S. Rho, Y. Yang, L.W.M.M. Terstappen, H. Gardeniers, S. Le Gac, P. Habibović, Programmable droplet-based microfluidic serial dilutor, J. Ind. Eng. Chem. 91 (2020) 231–239, https://doi.org/10.1016/j.jiec.2020.08.004.
[10] J. Wegrzyn, A. Samborski, L. Reissig, P.M. Korczyk, S. Blonski, P. Garstecki, Microfluidic architectures for efficient generation of chemistry gradations in droplets, Microfluid. Nanofluidics. 14 (2013) 235–245, https://doi.org/10.1007/s10404-012-1042-3.
[11] C.-G. Yang, Z.-R. Xu, A.P. Lee, J.-H. Wang, A microfluidic concentration-gradient droplet array generator for the production of multi-color nanoparticles, Lab. Chip. 13 (2013) 2815–2820, https://doi.org/10.1039/C3LC50254F.
[12] X. Niu, F. Gielen, J.B. Edel, A.J. deMello, A microdroplet dilutor for high-throughput screening, Nat. Chem. 3 (2011) 437–442, https://doi.org/10.1038/nchem.1046.
[13] P.M. Korczyk, L. Derzsi, S. Jakiela, P. Garstecki, Microfluidic traps for hard-wired operations on droplets, Lab. Chip. 13 (2013) 4096–4102, https://doi.org/10.1039/C3LC50347J.
[14] B. Bhattacharjee, S.A. Vanapalli, Electrocoalescence based serial dilution of microfluidic droplets, Biomicrofluidics. 8 (2014), 044111, https://doi.org/10.1063/1.4891775.
[15] J. Shemesh, T.B. Arye, J. Avesar, J.H. Kang, A. Fine, M. Super, A. Meller, D. E. Ingber, S. Levenberg, Stationary nanoliter droplet array with a substrate of choice for single adherent/nonadherent cell incubation and analysis, Proc. Natl. Acad. Sci. 111 (2014) 11293–11298, https://doi.org/10.1073/pnas.1404472111.
[16] M. Sun, S.S. Bithi, S.A. Vanapalli, Microfluidic static droplet arrays with tuneable gradients in material composition, Lab. Chip. 11 (2011) 3949, https://doi.org/10.1039/c1lc20709a.
[17] K. Totlani, J.-W. Hurkmans, W.M. van Gulik, M.T. Kreutzer, V. van Steijn, Scalable microfluidic droplet on-demand generator for non-steady operation of droplet-based assays, Lab. Chip. 20 (2020) 1398–1409, https://doi.org/10.1039/C9LC01103J.
[18] W. Postek, T.S. Kaminski, P. Garstecki, A precise and accurate microfluidic droplet dilutor, Analyst. 142 (2017) 2901–2911, https://doi.org/10.1039/C7AN00679A.
[19] E. Um, M.E. Rogers, H.A. Stone, Combinatorial generation of droplets by controlled assembly and coalescence, Lab. Chip. 13 (2013) 4674–4680, https://doi.org/10.1039/C3LC50957E.
[20] X. Niu, S. Gulati, J.B. Edel, A.J. deMello, Pillar-induced droplet merging in microfluidic circuits, Lab. Chip. 8 (2008) 1837, https://doi.org/10.1039/b813325e.
[21] K. Churski, T.S. Kaminski, S. Jakiela, W. Kamysz, W. Baranska-Rybak, D.B. Weibel, P. Garstecki, Rapid screening of antibiotic toxicity in an automated microdroplet system, Lab. Chip. 12 (2012) 1629–1637, https://doi.org/10.1039/C2LC21284F.
[22] K. Churski, P. Korczyk, P. Garstecki, High-throughput automated droplet microfluidic system for screening of reaction conditions, Lab. Chip. 10 (2010) 816–818.
[23] H. Babahosseini, T. Misteli, D.L. DeVoe, Microfluidic on-demand droplet generation, storage, retrieval, and merging for single-cell pairing, Lab. Chip. 19 (2019) 493–502, https://doi.org/10.1039/C8LC01178H.
[24] D. Cottinet, F. Condamine, N. Bremond, A.D. Griffiths, P.B. Rainey, J.A.G.M. de Visser, J. Baudry, J. Bibette, Lineage tracking for probing heritable phenotypes at single-cell resolution, PLOS ONE. 11 (2016), e0152395, https://doi.org/10.1371/journal.pone.0152395.
[25] P. Debski, K. Sklodowska, J. Michalski, P. Korczyk, M. Dolata, S. Jakiela, Continuous recirculation of microdroplets in a closed loop tailored for screening of bacteria cultures, Micromachines. 9 (2018) 469.
[26] K. Sklodowska, P. Debski, J. Michalski, P. Korczyk, M. Dolata, M. Zajac, S. Jakiela, Simultaneous measurement of viscosity and optical density of bacterial growth and death in a microdroplet, Micromachines. 9 (2018) 251, https://doi.org/10.3390/mi9050251.
[27] S. Jakiela, T.S. Kaminski, O. Cybulski, D.B. Weibel, P. Garstecki, Bacterial growth and adaptation in microdroplet chemostats, Angew. Chem. Int. Ed. 52 (2013) 8908–8911, https://doi.org/10.1002/anie.201301524.
[28] H.-H. Jeong, B. Lee, S.H. Jin, S.-G. Jeong, C.-S. Lee, A highly addressable static droplet array enabling digital control of a single droplet at pico-volume resolution, Lab. Chip. 16 (2016) 1698–1707, https://doi.org/10.1039/C6LC00212A.
[29] D. Zaremba, S. Blonski, M. Jachimek, M.J. Marijnissen, S. Jakiela, P.M. Korczyk, Investigations of modular microfluidic geometries for passive manipulations on droplets, Bull. Pol. Acad. Sci.-Tech. Sci. 66 (2018) 139–149, https://doi.org/10.24425/119068.
[30] J. Wang, J. Wang, L. Feng, T. Lin, Fluid mixing in droplet-based microfluidics with a serpentine microchannel, RSC Adv. 5 (2015) 104138–104144, https://doi.org/10.1039/C5RA21181F.
[31] D. Zaremba, S. Błoński, P.M. Korczyk, Integration of capillary–hydrodynamic logic circuitries for built-in control over multiple droplets in microfluidic networks, Lab. Chip. 21 (2021) 1771–1778, https://doi.org/10.1039/D0LC00900H.
[32] T.S. Kaminski, P. Garstecki, Controlled droplet microfluidic systems for multistep chemical and biological assays, Chem. Soc. Rev. 46 (2017) 6210–6226, https://doi.org/10.1039/C5CS00717H.